Spatiotemporal Sampling Trade-off for Inverse Diffusion Source Problems

John Murray-Bruce
Communications and Signal Processing Group
Electrical and Electronic Engineering Department
Imperial College London
e-mail: john.murray-bruce07@imperial.ac.uk

Pier Luigi Dragotti
Communications and Signal Processing Group
Electrical and Electronic Engineering Department
Imperial College London
e-mail: p.dragotti@imperial.ac.uk

***Abstract*—We consider the spatiotemporal sampling of diffusion fields induced by M point sources, and study the associated inverse problem of recovering the initial parameters of the unknown sources. In particular, we focus on characterising qualitatively the error of the obtained source estimates. To achieve this, we obtain an expression with which we can trade the sensor density for performance accuracy. In other words, by evaluating the optimal sampling instant for a given sensor density—and using the corresponding field samples at that instant—we can expect to obtain an improvement in the estimation performance when compared to an arbitrary sampling instant. Finally, several numerical simulations are presented, to support the theoretical results obtained.**

I. Introduction

Diffusion is defined as the movement of particles from regions of high concentrations to regions of lower concentrations, until an equilibrium is established. Of huge importance is its role as an accurate model for the transport mechanism behind many naturally occurring phenomena. For example, it models the evolution of the thermal field when a heat source is applied to a conducting medium [1], the spreading of fungal diseases in precision agriculture [2], as well as the propagation of bio-chemical substances and leakages in environmental monitoring [3]. In these examples, and beyond, a robust approach for recovering the source given measurements of the field has been a topic of great interest.

In a recent work [4], an efficient solution to the inverse source problem (ISP) for a class of linear partial differential equations (PDEs) was proposed. In that approach, a sequence of general measurements is computed from a specific family of weighted linear sums of the field samples. Specifically, the desired sequence of weights, in the sums, are those that reproduce a family of exponentials from weighted and summed translates of the Green's function for the underlying field's PDE model. Under this condition, the sequence of generalised measurements obtained are of a Prony-type system, from which we can recover the unknown sources.

The aim of this work is to analyse the accuracy of that approach for diffusion fields. First we argue that performance, given noiseless sensor measurements, is linked to the accuracy of the exponential reproduction step. In other words, picking coefficients that accurately reproduce exponentials means reliable source estimates can be obtained. Therefore by investigating the error associated with the function approximation, we aim to gain a better understanding of how to achieve the best estimation performance for a given sensor density. The answer to such a question is paramount when designing a sensor network for environmental monitoring [5], [6].

This remainder of this paper has been divided into four main parts. First, we present an overview of the framework for solving inverse diffusion source problems in Section II. We then derive the desired error expressions in Section III and present numerical results in Section IV to reinforce our approach. The paper is then concluded in Section V.

II. Solving the inverse diffusion source problem

Mathematically a diffusion field $u(\mathbf{x},t)$ over space and time, induced by a source distribution $f(\mathbf{x})\delta(t)$, is governed by:

$$\frac{\partial}{\partial t}u(\mathbf{x},t) = \mu\nabla^2 u(\mathbf{x},t) + f(\mathbf{x})\delta(t),$$

where μ is the diffusivity of the medium and $\delta(t)$ is the Dirac delta distribution. Under a Sommerfeld radiation condition, it can be shown that the Green's function for this PDE is [7],

$$g(\mathbf{x},t) = \frac{1}{(4\pi\mu t)^{d/2}} e^{-\frac{\|\mathbf{x}\|^2}{4\mu t}} H(t), \tag{1}$$

where $d = \{1,2,3\}$ is used to indicate the number of spatial dimensions—one, two or three, respectively—and $H(t)$ is the unit step function. Consequently, the solution to the forward problem may be written as:

$$u(\mathbf{x},t) = g(\mathbf{x},t) * f(\mathbf{x}) = \int_{\mathbf{x}'\in\mathbb{R}^d} g(\mathbf{x}-\mathbf{x}',t) f(\mathbf{x}')\mathrm{d}\mathbf{x}'.$$

The goal of the inverse diffusion source problem (IDSP) is then to recover $f(\mathbf{x})$ from a sequence of sensor measurements $\{\varphi_{n,l}\}_{\boldsymbol{n}}$ of the diffusion field $u(\mathbf{x},t)$, where $\varphi_{\boldsymbol{n},l} = u(\mathbf{x}_{\boldsymbol{n}}, t_l)$ is the field sample obtained at time instant $t = t_l$ by the sensor located at $\mathbf{x} = \mathbf{x}_{\boldsymbol{n}} = \boldsymbol{n}\boldsymbol{\Delta}_{\mathbf{x}}$, wherein we have used the multi-index notation $\boldsymbol{n} = (n_1,\ldots,n_d)$, and the sensor spacing in each dimension is denoted by $\boldsymbol{\Delta}_{\mathbf{x}} = (\Delta_1,\ldots,\Delta_d)$. Finally, for notational simplicity we write $\boldsymbol{n}\boldsymbol{\Delta}_{\mathbf{x}} = (n_1\Delta_1,\ldots,n_d\Delta_d)$.

Our focus herein, will be on the recovery of source distributions, $f(\mathbf{x})$, which can be modelled as a superposition of M Dirac deltas, i.e.

$$f(\mathbf{x}) = \sum_{m=1}^{M} c_m \delta(\mathbf{x} - \boldsymbol{\xi}_m). \tag{2}$$

Due to this parametrisation, i.e. Equation (2), recovering $f(\mathbf{x})$ amounts to finding the M pairs $\{(c_m, \xi_m)\}_m$. Note that, although we focus on point sources, the framework can also be applied to non-localized sources, such as convex polygonal sources [8] or more generally sources whose spatial support can be described by an FRI curve model [9]. We defer the explicit treatment of the estimation errors for such sources to future works in the area.

A. Source recovery framework: a review

We now outline the framework formally presented by the authors in [4], [10], where it was shown that the unknown source parameters, i.e. $\{c_m, \boldsymbol{\xi}_m\}_{m=1}^M$ in (2), can be recovered from the multidimensional sequence[1],

$$\mathcal{R}(\boldsymbol{k}) \stackrel{\text{def}}{=} \langle f(\mathbf{x}), \Psi_{\boldsymbol{k}}(\mathbf{x}) \rangle_{\mathbf{x} \in \mathbb{R}^d}, \tag{3}$$

by using multidimensional variations of Prony's method [11], if $\Psi_{\boldsymbol{k}}(\mathbf{x})$ is carefully chosen to be the multidimensional imaginary exponential $\Psi_{\boldsymbol{k}}(\mathbf{x}) = e^{\mathrm{j}\boldsymbol{k}\cdot\mathbf{x}}$, where $\boldsymbol{k} \in \mathbb{Z}^d$. To see this, observe that substituting $\Psi_{\boldsymbol{k}}(\mathbf{x}) = e^{\mathrm{j}\boldsymbol{k}\cdot\mathbf{x}}$ into (3) yields

$$\mathcal{R}(\boldsymbol{k}) = \sum_{m=1}^{M} c_m e^{\mathrm{j}\boldsymbol{k}\cdot\boldsymbol{\xi}_m}. \tag{4}$$

Hence according to (4), $\mathcal{R}(\boldsymbol{k})$ is governed by a power-sum series. This system can thus be solved for $\{c_m, \boldsymbol{\xi}_m\}_{m=1}^M$, given access to the exact multidimensional sequence $\{\mathcal{R}(\boldsymbol{k})\}_{\boldsymbol{k}=\mathbf{0}}^{\boldsymbol{K}}$ where $\boldsymbol{K} = (K_1, K_2, \ldots, K_d)$ and $K_i \geq 2M - 1$ for all $i = 1, 2, \ldots, d$ (see [4], [11], [12]).

Moreover, the sequence (4) can be evaluated from linear combinations of the sensor measurements. Specifically, for

$$\sum_{\boldsymbol{n} \in \mathbb{Z}^d} w_{\boldsymbol{n}}(\boldsymbol{k}, l) \varphi_{\boldsymbol{n},l} = \mathcal{R}(\boldsymbol{k}), \tag{5}$$

to hold true, then it must be required:

$$\sum_{\boldsymbol{n} \in \mathbb{Z}^d} w_{\boldsymbol{n}}(\boldsymbol{k}, l) g(\mathbf{x}_{\boldsymbol{n}} - \mathbf{x}, t_l) = \Psi_{\boldsymbol{k}}(\mathbf{x}). \tag{6}$$

Naturally, it is necessary to understand whether the so called exponential reproduction problem—when $\Psi_{\boldsymbol{k}}(\mathbf{x}) = e^{\mathrm{j}\boldsymbol{k}\cdot\mathbf{x}}$ in (6)—is at all possible. To this end, by leveraging from certain results in function approximation theory, it can be shown that (6) is exact if and only if $g(\mathbf{x}, t_l)$ satisfies the generalised Strang-Fix conditions [4], [13], [14]:

$$G(-\mathrm{j}\boldsymbol{k}, t_l) \neq 0 \quad \text{and} \tag{7}$$

$$G(-\mathrm{j}\boldsymbol{k} + \mathrm{j}2\pi\boldsymbol{\ell}/\boldsymbol{\Delta}_{\mathbf{x}}, t_l) = 0 \quad \forall \boldsymbol{\ell} \in \mathbb{Z}^d \backslash \{\mathbf{0}\}, \tag{8}$$

[1]The inner product here is the usual one defined on L^2, i.e. the space of square-integrable functions.

where $G(\mathbf{s}, t_l) = \int_{\mathbf{x} \in \mathbb{R}^d} g(\mathbf{x}, t_l) e^{-\mathbf{s}\cdot\mathbf{x}} \mathrm{d}\mathbf{x}$ is the multidimensional (spatial) Laplace transform of $g(\mathbf{x}, t_l)$. However, when $g(\mathbf{x}, t_l)$ does not satisfy the Strang-Fix conditions—as in the case of the Green's function (1)—it has been shown that an approximate exponential reproduction can be achieved [15]. In particular provided G decays fast enough, the coefficients

$$w_{\boldsymbol{n}}(\boldsymbol{k}, l) = \prod_{i=1}^{d} \Delta_{x_i} \frac{e^{\mathrm{j}\boldsymbol{k}\cdot(\boldsymbol{n}\boldsymbol{\Delta}_{\mathbf{x}})}}{G(-\mathrm{j}\boldsymbol{k}, t_l)}, \tag{9}$$

provides a good approximation to $\Psi_{\boldsymbol{k}}(\mathbf{x})$ [15], i.e.

$$\hat{\Psi}_{\boldsymbol{k}}(\mathbf{x}, t_l) \stackrel{\text{def}}{=} \sum_{\boldsymbol{n} \in \mathbb{Z}^d} w_{\boldsymbol{n}}(\boldsymbol{k}, l) g(\boldsymbol{n}\boldsymbol{\Delta}_{\mathbf{x}} - \mathbf{x}, t_l) \approx \Psi_{\boldsymbol{k}}(\mathbf{x}). \tag{10}$$

Remark 1: The approximation of $\Psi_{\boldsymbol{k}}(\mathbf{x})$ with $\hat{\Psi}_{\boldsymbol{k}}(\mathbf{x}, t_l)$ depends on the choice of coefficients $w_{\boldsymbol{n}}(\boldsymbol{k}, l)$. For instance, besides (9) there exists coefficients that ensures a minimum L_2-norm approximation of $\Psi_{\boldsymbol{k}}(\mathbf{x})$ [16], whilst another choice exists which ensures that $\hat{\Psi}_{\boldsymbol{k}}(\mathbf{x}, t_l)$ interpolates $\Psi_{\boldsymbol{k}}(\mathbf{x})$, i.e. they coincide at $\mathbf{x} = \mathbf{x}_{\boldsymbol{n}}$ [16]. However, the coefficients (9) is obtained by simply assuming that the second requirement of the Strang-Fix condition (8) is approximately satisfied, meaning $G(-\mathrm{j}\boldsymbol{k} + \mathrm{j}2\pi\boldsymbol{\ell}/\boldsymbol{\Delta}_{\mathbf{x}}, t_l) \approx 0$, $\forall \boldsymbol{\ell} \in \mathbb{Z}^d \backslash \{\mathbf{0}\}$. We will see later on that $G(\mathbf{s}, t_l)$ decays exponentially fast with $\boldsymbol{\ell}$, for $\mathbf{s} = -\mathrm{j}\boldsymbol{k} + \mathrm{j}2\pi\boldsymbol{\ell}/\boldsymbol{\Delta}_{\mathbf{x}}$. Qualitatively speaking—if Strang-Fix is not exactly satisfied—demanding a fast decay will give a better approximation.

This paper aims to study the accuracy of this approximation in the specific IDSP set up; in so doing, we will be able to:

1) Understand the extent of the average error introduced in the computation of the sequence $\mathcal{R}(\boldsymbol{k})$, and;
2) Optimise the sampling instant for a fixed topology when solving the IDSP, by choosing a t_l that minimises the average approximation error.

III. Exponential Approximation using Translates of the Green's Function

Note that solving the inverse source problem using the framework above involves three simple steps:

1) Find the exponential reproducing coefficients $w_{n,l}(\boldsymbol{k})$;
2) Using these coefficients, and the spatial sensor samples, compute the sequence $\mathcal{R}(\boldsymbol{k})$ using (5), and;
3) Estimate the desired source parameters from $\{\mathcal{R}(\boldsymbol{k})\}_{\boldsymbol{k}}$ using multidimensional Prony-like methods.

By studying (3) and also recalling that $f(\mathbf{x})$ is a superposition of highly localised Dirac delta distributions, we can conclude that (in addition to the effect of sensor noise) the errors in the terms of $\{\mathcal{R}(\boldsymbol{k})\}$ is directly dependent on the pointwise accuracy of the exponential reproduction. Specifically, if the pointwise errors of the exponentials reproduced by using (6) at the precise source locations are large, so too will the error in $\{\mathcal{R}(\boldsymbol{k})\}_{\boldsymbol{k}}$, and *vice versa* for small errors.

Consequently in order to understand, at least qualitatively, the errors in the estimates of $f(\mathbf{x})$ from employing the framework outlined in the previous section, it is useful to

characterise the average approximation error obtained when we use $\hat{\Psi}_{\boldsymbol{k}}(\mathbf{x}, t_l)$ as an approximation for $\Psi_{\boldsymbol{k}}(\mathbf{x})$. Let

$$\epsilon_{\boldsymbol{k}}(\mathbf{x}, t_l) = \Psi_{\boldsymbol{k}}(\mathbf{x}) - \hat{\Psi}_{\boldsymbol{k}}(\mathbf{x}, t_l),$$

then by noting that $w_{\boldsymbol{n}}(\boldsymbol{k}, l) = w_{\mathbf{0}}(\boldsymbol{k}, l)e^{\mathrm{j}\boldsymbol{k}\cdot(\boldsymbol{n}\boldsymbol{\Delta}_{\mathbf{x}})}$ and writing the approximation for (6) as

$$\hat{\Psi}_{\boldsymbol{k}}(\mathbf{x}, t_l) = e^{\mathrm{j}\boldsymbol{k}\cdot\mathbf{x}} \sum_{\boldsymbol{n}} w_{\mathbf{0}}(\boldsymbol{k}, l)e^{\mathrm{j}\boldsymbol{k}\cdot(\boldsymbol{n}\boldsymbol{\Delta}_{\mathbf{x}}-\mathbf{x})} g(\boldsymbol{n}\boldsymbol{\Delta}_{\mathbf{x}} - \mathbf{x}, t_l),$$

finally leads to the following expression:

$$\epsilon_{\boldsymbol{k}}(\mathbf{x}, t_l) = e^{\mathrm{j}\boldsymbol{k}\cdot\mathbf{x}} \left(1 - w_{\mathbf{0}}(\boldsymbol{k}, l) \sum_{\boldsymbol{n}} e^{\mathrm{j}\boldsymbol{k}\cdot(\boldsymbol{n}\boldsymbol{\Delta}_{\mathbf{x}}-\mathbf{x})} g(\boldsymbol{n}\boldsymbol{\Delta}_{\mathbf{x}} - \mathbf{x}, t_l)\right).$$

Then the average approximation error,

$$\begin{aligned}
E_{\boldsymbol{k}}(t_l) &= \int_{\mathbf{x}} |\epsilon_{\boldsymbol{k}}(\mathbf{x}, t_l)|^2 \, \mathrm{d}\mathbf{x} \\
&= \int_{\mathbf{x}} \left| 1 - w_{\mathbf{0}}(\boldsymbol{k}, l) \sum_{\boldsymbol{n}} e^{\mathrm{j}\boldsymbol{k}\cdot(\boldsymbol{n}\boldsymbol{\Delta}_{\mathbf{x}}-\mathbf{x})} g(\boldsymbol{n}\boldsymbol{\Delta}_{\mathbf{x}} - \mathbf{x}, t_l) \right|^2 \mathrm{d}\mathbf{x} \\
&= \int_{\mathbf{x}} \left| 1 - \frac{w_{\mathbf{0}}(\boldsymbol{k}, l)}{\prod_i \Delta_{x_i}} \sum_{\boldsymbol{\ell}} G(2\pi\mathrm{j}\frac{\boldsymbol{\ell}}{\boldsymbol{\Delta}_{\mathbf{x}}} - \mathrm{j}\boldsymbol{k}, t_l) e^{-2\pi\mathrm{j}\frac{\boldsymbol{\ell}}{\boldsymbol{\Delta}_{\mathbf{x}}}\cdot\mathbf{x}} \right|^2 \mathrm{d}\mathbf{x} \\
&= \int_{\mathbf{x}} \left| 1 - \frac{1}{G(-\mathrm{j}\boldsymbol{k}, t_l)} \sum_{\boldsymbol{\ell}} G(2\pi\mathrm{j}\frac{\boldsymbol{\ell}}{\boldsymbol{\Delta}_{\mathbf{x}}} - \mathrm{j}\boldsymbol{k}, t_l) e^{-\mathrm{j}2\pi\frac{\boldsymbol{\ell}}{\boldsymbol{\Delta}_{\mathbf{x}}}\cdot\mathbf{x}} \right|^2 \mathrm{d}\mathbf{x},
\end{aligned}$$

where the penultimate equality follows by applying the Poisson summation formula, whilst the last follows by substituting $w_{\mathbf{0}}(\boldsymbol{k}, l) = \frac{\prod_i \Delta_{x_i} e^{\mathrm{j}\boldsymbol{k}\cdot(\boldsymbol{n}\boldsymbol{\Delta}_{\mathbf{x}})}}{G(-\mathrm{j}\boldsymbol{k}, t_l)}$.

Lemma 1 (Laplace transform of $g(\mathbf{x}, t_l)$ [4]): The bi-lateral Laplace transform of the Green's function (1) is:

$$G(\mathbf{s}, t_l) = e^{\mu t_l \|\mathbf{s}\|^2}. \tag{11}$$

Before proceeding we observe that, by putting $\mathbf{s} = -\mathrm{j}\boldsymbol{k} + \mathrm{j}2\pi\boldsymbol{\ell}/\boldsymbol{\Delta}_{\mathbf{x}}$ into (11), as previously mentioned G does indeed decay exponentially fast, with $\|\boldsymbol{\ell}\|^2$.

Now substituting (11) into the above expression for $E_{\boldsymbol{k}}(t_l)$ produces

$$\begin{aligned}
E_{\boldsymbol{k}}(t_l) &= \int_{\mathbf{x}} \left| 1 - e^{\mu t_l \|\boldsymbol{k}\|^2} \sum_{\boldsymbol{\ell}\in\mathbb{Z}^d} e^{-\mu t_l \|2\pi(\boldsymbol{\ell}/\boldsymbol{\Delta}_{\mathbf{x}}) - \boldsymbol{k}\|^2 - \mathrm{j}2\pi\frac{\boldsymbol{\ell}}{\boldsymbol{\Delta}_{\mathbf{x}}}\cdot\mathbf{x}} \right|^2 \mathrm{d}\mathbf{x} \\
&= \int_{\mathbf{x}} \left| 1 - \sum_{\boldsymbol{\ell}} e^{-\mu t_l \|2\pi(\boldsymbol{\ell}/\boldsymbol{\Delta}_{\mathbf{x}})\|^2 - 4\pi(\boldsymbol{\ell}/\boldsymbol{\Delta}_{\mathbf{x}})\cdot\boldsymbol{k} - \mathrm{j}2\pi\frac{\boldsymbol{\ell}}{\boldsymbol{\Delta}_{\mathbf{x}}}\cdot\mathbf{x}} \right|^2 \mathrm{d}\mathbf{x} \\
&= \int_{\mathbf{x}} \left| 1 - \sum_{\boldsymbol{\ell}} \alpha_{\boldsymbol{k}}(\boldsymbol{\ell}, t_l) e^{-\mathrm{j}2\pi\frac{\boldsymbol{\ell}}{\boldsymbol{\Delta}_{\mathbf{x}}}\cdot\mathbf{x}} \right|^2 \mathrm{d}\mathbf{x}.
\end{aligned}$$

Therefore,

$$E_{\boldsymbol{k}}(t_l) = \int_{\mathbf{x}} 1 + \sum_{\boldsymbol{\ell}} \left(\beta_{\boldsymbol{k}}(\boldsymbol{\ell}, t_l) - \alpha_{\boldsymbol{k}}(\boldsymbol{\ell}, t_l) - \alpha_{\boldsymbol{k}}(-\boldsymbol{\ell}, t_l)\right) e^{\mathrm{j}2\pi\frac{\boldsymbol{\ell}}{\boldsymbol{\Delta}_{\mathbf{x}}}\cdot\mathbf{x}} \mathrm{d}\mathbf{x}, \tag{12}$$

where,

$$\begin{aligned}
\alpha_{\boldsymbol{k}}(\boldsymbol{\ell}, t_l) &= e^{-\mu t_l \|2\pi(\boldsymbol{\ell}/\boldsymbol{\Delta}_{\mathbf{x}})\|^2 - 4\pi(\boldsymbol{\ell}/\boldsymbol{\Delta}_{\mathbf{x}})\cdot\boldsymbol{k}} \\
\beta_{\boldsymbol{k}}(\boldsymbol{\ell}, t_l) &= \sum_{\bar{\boldsymbol{\ell}}} \alpha_{\boldsymbol{k}}(\bar{\boldsymbol{\ell}}) \alpha_{\boldsymbol{k}}(\boldsymbol{\ell} - \bar{\boldsymbol{\ell}}).
\end{aligned}$$

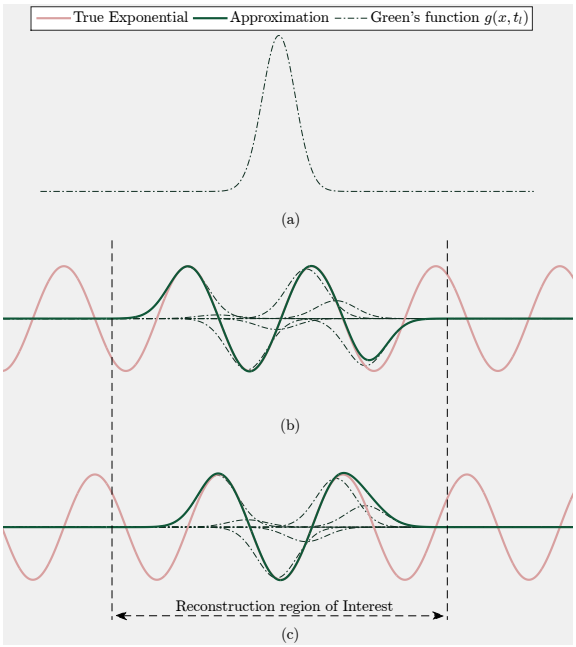

Fig. 1. Exponential reproduction using uniform translates of 1-D Gaussian prototype function $g(\mathbf{x}, t_l)$, shown in (a). The reproduced exponential is $e^{\mathrm{j}9x}$, i.e. $k = 9$, using $\Delta_x = 0.15$ and $t_l = 60$. (b) $\Re\{e^{\mathrm{j}9x}\}$, and (c) $\Im\{e^{\mathrm{j}9x}\}$. The dashed curves show the shifted and weighted versions of $g(\mathbf{x}, t_l)$.

This expression may be evaluated numerically over several values of t_l for fixed $\boldsymbol{k}$ and $\boldsymbol{\Delta}_{\mathbf{x}}$. Since the summations in (12) are over infinite number of terms, in order to make proper use of (12), its convergence properties must be understood. However by incorporating the interesting fact that: for the sensor network applications, $\boldsymbol{n} = \mathbf{0}, \ldots, \boldsymbol{N}$ is finite and by virtue, so are the sums in (5) and (10). In the next section, we study the case where the summation in (5) (and (10)) in finite.

A. The finite sum case

In reality, since the number of sensors used is finite the exponential reconstruction is only local. This is easily seen by observing that, in (10), we are only summing weighted translates of the Green's function centred at the sensor locations. Hence the approximation $\hat{\Psi}_{\boldsymbol{k}}(\mathbf{x}, t_l)$ will be effectively zero outside a certain interval, especially since $g(\mathbf{x}, t_l)$ has fast decay. We show a 1-D illustration of this in Figure 1, the Gaussian prototype function (and translates) decay rapidly and so does $\hat{\Psi}_{\boldsymbol{k}}(\mathbf{x}, t_l)$ outside the region of interest. This therefore motivates our study of the approximation error, over a specific region of interest, for example the region enclosed by the convex hull of the sensor locations, i.e. the interior of the d-cube $\Omega = [0, X_1] \times [0, X_2] \times \cdots \times [0, X_d]$. Under this new set up, the square absolute error can be derived as shown in the following proposition.

Proposition 1: The approximation error for the exponential

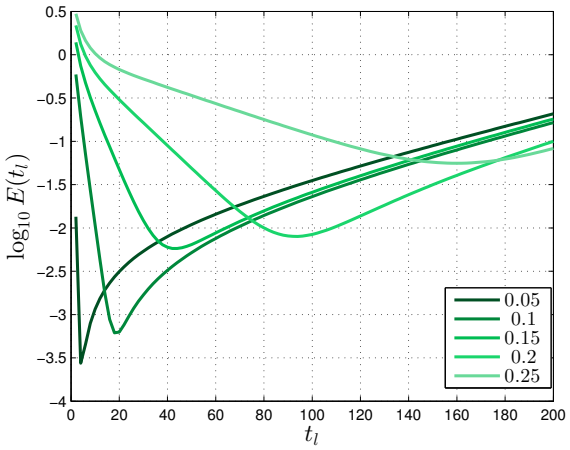

Fig. 2. The variation of the average approximation error over the interval $x \in [0, 2]$ using $k = 10$, we show plots for several values of Δ_x and for $t_l \in [0, 200]$.

approximation problem (10) using the coefficients (9) is:

$$|\epsilon_{\boldsymbol{k}}(\mathbf{x}, t_l)|^2 = 1 - \frac{2\prod_{i=1}^{d}\Delta_{x_i}}{e^{-\mu t_l\|\boldsymbol{k}\|^2}}\sum_{\boldsymbol{n}=\mathbf{0}}^{\boldsymbol{N}} g_{\boldsymbol{n}}\cos\left(\boldsymbol{k}\cdot(\boldsymbol{n}\boldsymbol{\Delta}_{\mathbf{x}} - \mathbf{x})\right) + \frac{\prod_{i=1}^{d}\Delta_{x_i}^2}{e^{-2\mu t_l\|\boldsymbol{k}\|^2}}\left(2\sum_{\boldsymbol{n}=\mathbf{1}}^{\boldsymbol{N}} b_{\boldsymbol{n}}\cos\left(\boldsymbol{k}\cdot\boldsymbol{n}\boldsymbol{\Delta}_{\mathbf{x}}\right) + b_{\mathbf{0}}\right),$$

where we use $g_{\boldsymbol{n}} = g(\boldsymbol{n}\boldsymbol{\Delta}_{\mathbf{x}} - \mathbf{x}, t_l)$, $b_{\boldsymbol{n}} = \sum_{\bar{\boldsymbol{n}}=\boldsymbol{n}}^{\boldsymbol{N}} g_{\bar{\boldsymbol{n}}-\boldsymbol{n}}g_{\bar{\boldsymbol{n}}}$ and $g_{\bar{\boldsymbol{n}}-\boldsymbol{n}}g_{\bar{\boldsymbol{n}}} = \frac{1}{(4\pi\mu t_l)^d}e^{\frac{\|\boldsymbol{n}\boldsymbol{\Delta}_{\mathbf{x}}\|^2}{4\mu t_l}}e^{-\frac{\|(\bar{\boldsymbol{n}}-\boldsymbol{n}/2)\boldsymbol{\Delta}_{\mathbf{x}}-\mathbf{x}\|^2}{2\mu t_l}}$.

Proof: From $|\epsilon_{\boldsymbol{k}}(\mathbf{x}, t_l)|^2 = \epsilon_{\boldsymbol{k}}(\mathbf{x}, t_l)\epsilon^*_{\boldsymbol{k}}(\mathbf{x}, t_l)$, it follows that:

$$|\epsilon_{\boldsymbol{k}}(\mathbf{x}, t_l)|^2 = \left|e^{\mathrm{j}\boldsymbol{k}\cdot\mathbf{x}} - \frac{\prod_i \Delta_{x_i}}{G(-\mathrm{j}\boldsymbol{k})}\sum_{\boldsymbol{n}=\mathbf{0}}^{\boldsymbol{N}} e^{\mathrm{j}\boldsymbol{k}\cdot(\boldsymbol{n}\boldsymbol{\Delta}_{\mathbf{x}})}g_{\boldsymbol{n}}\right|^2,$$

from this we can then derive the following expansion,

$$|\epsilon_{\boldsymbol{k}}(\mathbf{x}, t_l)|^2 = 1 - \frac{\prod_{i=1}^{d}\Delta_{x_i}}{e^{-\mu t_l\|\boldsymbol{k}\|^2}}\sum_{\boldsymbol{n}=\mathbf{0}}^{\boldsymbol{N}} g_{\boldsymbol{n}}\left(e^{\mathrm{j}\boldsymbol{k}\cdot(\boldsymbol{n}\boldsymbol{\Delta}_{\mathbf{x}}-\mathbf{x})} + e^{\mathrm{j}\boldsymbol{k}\cdot(\mathbf{x}-\boldsymbol{n}\boldsymbol{\Delta}_{\mathbf{x}})}\right) + \frac{\prod_{i=1}^{d}\Delta_{x_i}^2}{e^{-2\mu t_l\|\boldsymbol{k}\|^2}}\left(\sum_{\boldsymbol{n}=\mathbf{0}}^{\boldsymbol{N}} e^{\mathrm{j}\boldsymbol{k}\cdot\boldsymbol{n}\boldsymbol{\Delta}_{\mathbf{x}}}g_{\boldsymbol{n}}\right)\left(\sum_{\boldsymbol{n}=\mathbf{0}}^{\boldsymbol{N}} e^{-\mathrm{j}\boldsymbol{k}\cdot\boldsymbol{n}\boldsymbol{\Delta}_{\mathbf{x}}}g_{\boldsymbol{n}}\right).$$

Finally by using the fact that $2\cos(x) = e^{\mathrm{j}x} + e^{-\mathrm{j}x}$ and by applying the discrete convolution formula to the sums in the last term, we obtain,

$$|\epsilon_{\boldsymbol{k}}(\mathbf{x}, t_l)|^2 = 1 - \frac{2\prod_{i=1}^{d}\Delta_{x_i}}{e^{-\mu t_l\|\boldsymbol{k}\|^2}}\sum_{\boldsymbol{n}=\mathbf{0}}^{\boldsymbol{N}} g_{\boldsymbol{n}}\cos\left(\boldsymbol{k}\cdot(\boldsymbol{n}\boldsymbol{\Delta}_{\mathbf{x}}-\mathbf{x})\right) + \frac{\prod_{i=1}^{d}\Delta_{x_i}^2}{e^{-2\mu t_l\|\boldsymbol{k}\|^2}}\left(\sum_{\boldsymbol{n}=\mathbf{1}}^{\boldsymbol{N}} b_{\boldsymbol{n}}\left(e^{\mathrm{j}\boldsymbol{k}\cdot\boldsymbol{n}\boldsymbol{\Delta}_{\mathbf{x}}} + e^{-\mathrm{j}\boldsymbol{k}\cdot\boldsymbol{n}\boldsymbol{\Delta}_{\mathbf{x}}}\right) + \sum_{\boldsymbol{n}=\mathbf{0}}^{\boldsymbol{N}} g_{\boldsymbol{n}}^2\right).$$

From here, the required result follows immediately. ∎

Then the average error $E_{\boldsymbol{k}}(t_l) = \int_{\mathbf{x}\in\Omega}|\epsilon_{\boldsymbol{k}}(\mathbf{x}, t_l)|^2 \mathrm{d}\mathbf{x}$ can be computed using numerical techniques.

TABLE I
ESTIMATED SOURCE PARAMETERS (c_1, ξ_1) FOR SOME (Δ_x, t_l)-PAIRS. THE EXPONENTIALS USED HERE ARE $\{e^{\mathrm{j}kx}\}$ FOR $k = 9, 10$.

		Δ_x		
		0.05	0.15	0.20
t_l	4	(0.99975, 1.78613)	(1.00710, 1.80000)	(1.00710, 1.80000)
	40	(1.00030, 1.78550)	(1.01182, 1.79325)	(1.05116, 1.80416)
	90	(1.00874, 1.79835)	(1.00459, 1.79921)	(1.03292, 1.80201)

IV. NUMERICAL SIMULATIONS

A. Single source simulations

In the following simulations, we study the 1-D set-up because its numerical results are relatively easier to present graphically. First we provide plots, in Figure 2, of the behaviour of the average error over a finite region $x \in [0, 2]$, as the sampling instant t_l increases. Each line in Figure 2 corresponds to a value of specific sensor spacing value $\Delta_x \in \{0.05, 0.1, 0.15, 0.2, 0.25\}$ for a fixed $k = 10$. As expected we can observe that the average error $E_k(t_l) = \int_x |\epsilon_k(x, t_l)|^2 dx$ is a convex function. Moreover as Δ_x increases, so does the minimum average error $E_k(t_l^\circ)$ and its location t_l°.

TABLE II
LOCATION ESTIMATION ERRORS FOR SOME (Δ_x, t_l)-PAIRS. THE EXPONENTIALS USED HERE ARE $\{e^{\mathrm{j}kx}\}$ FOR $k = 9, 10$.

		Δ_x		
		0.05	0.10	0.15
t_l	4	0.01329	0.07669	0.11952
	20	0.05345	0.03100	0.06979
	40	0.09295	0.06380	0.03267

1) Estimation error: We now simulate a single source diffusion field in 1-D with $(c_1, \xi_1) = (1, 1.785s)$ and examine the error in the source estimates, when the field is sampled using a sensor network with spacing $\Delta_x = \{0.05, 0.15, 0.20\}m$ and time instant $t_l = \{4, 40, 90\}s$. For each sensor spacing-sampling instant pair, we obtain the diffusion field samples and estimate (c_1, ξ_1) using the approach in Section II.

We show the normalized absolute error (i.e. $|\xi_1 - \hat{\xi}_1|/\xi_1$) of the location estimates in Table II. This result is obtained by averaging the errors obtained over $20,000$ independent trials, where each trial uses a new source location drawn uniformly at random from the interval $[0, 2]m$. In line with expectation, we notice that the setup having $(\Delta_x, t_l) = (0.05m, 4s)$ produces the smallest error on average.

B. Multiple source simulations

In this section, we perform further numerical investigations using a multiple source diffusion field. We consider the diffusion field induced by four (i.e. $M = 4$) sources and investigate the estimation performance in such a scenario.

Guided by the plot Figure 2 and noting that $\Delta_x = 0.2$, to achieve a good reconstruction we should choose $t_l \in [80, 110]$. For comparison, we show the recovered estimates for $t_l = \{20, 80\}$ in Figure 3. Specifically Figure 3(a) shows a successful recovery when $t_l = 80$, for all four diffusion

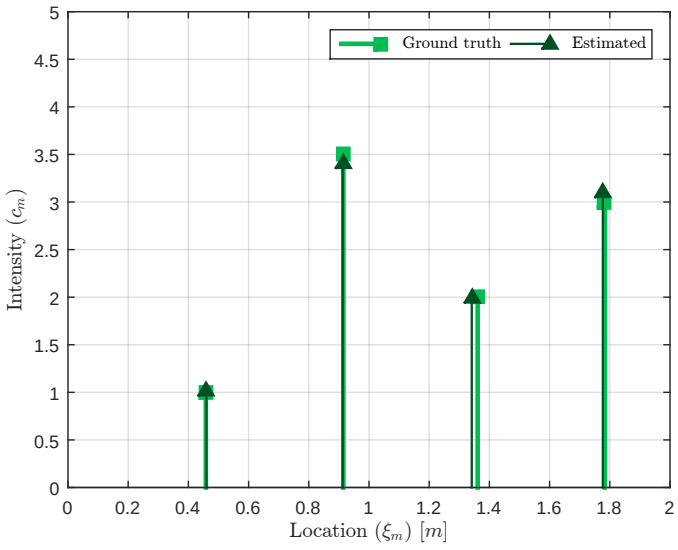

(a)

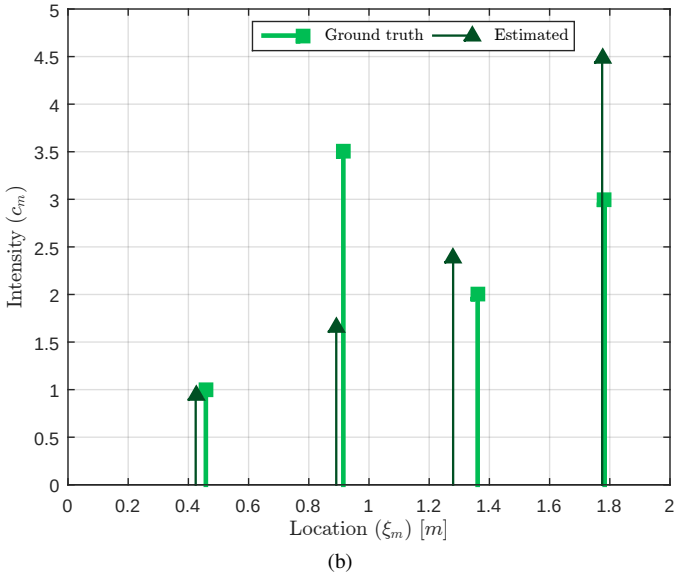

(b)

Fig. 3. Recovery of multiple diffusion sources from the field samples taken with sensors separated by $\Delta_x = 0.2m$. The true source locations and intensities are depicted by the locations and heights, respectively, of the stems. Eight consecutive generalised measurements, i.e. $\{\mathcal{R}(k)\}_{k=-4}^{3}$, have been used as required by Prony's method (and its variations). In (a) we show reliable recovery of the estimates by using $t_l = 80$, whilst in (b) the sampling instant $t_l = 20$ has been used leading to less reliable source estimates.

sources, in contrast to a diminished estimation accuracy when $t_l = 20$.

V. Conclusion

In this paper we have overviewed a recent method for solved inverse diffusion source problems. Then we investigated the associated error in the estimated source parameters by using the exponential reproduction approximation error as a suitable proxy for this. With the obtained expression the optimal sampling instant for a given sensor density can be computed. Moreover, it can also be useful when designing sampling strategies by trading off number of sensors for estimation performance.

Acknowledgment

This work is supported by the European Research Council (ERC) starting investigator award Nr. 277800 (RecoSamp).

References

[1] J. Murray-Bruce and P. L. Dragotti, "Estimating localized sources of diffusion fields using spatiotemporal sensor measurements," *IEEE Transactions on Signal Processing*, vol. 63, no. 12, pp. 3018–3031, June 2015.

[2] K. Langendoen, A. Baggio, and O. Visser, "Murphy loves potatoes: experiences from a pilot sensor network deployment in precision agriculture," in *Proc. 20th International Parallel and Distributed Processing Symposium (IPDPS'06)*, April 2006, p. 8.

[3] J. Matthes, L. Gröll, and H. B. Keller, "Source localization by spatially distributed electronic noses for advection and diffusion," *IEEE Transactions on Signal Processing*, vol. 53, no. 5, pp. 1711–1719, May 2005.

[4] J. Murray-Bruce and P. L. Dragotti, "A universal sampling framework for solving physics-driven inverse source problems," 2016, submitted.

[5] A. Aldroubi, C. Cabrelli, U. Molter, and S. Tang, "Dynamical sampling," *Applied and Computational Harmonic Analysis*, 2015.

[6] J. Ranieri, Y. Lu, A. Chebira, and M. Vetterli, "Sampling and Reconstructing Diffusion Fields with Localized Sources," in *Proc. IEEE International Conference on Acoustics, Speech, And Signal Processing (ICASSP'11)*. Prague, Czech Republic: IEEE Service Center, NJ, USA, May 2011, pp. 4016–4019.

[7] D. G. Duffy, *Greens functions with applications*. Chapman and Hall/CRC Press, 2001.

[8] J. Murray-Bruce and P. L. Dragotti, "Reconstructing non-point sources of diffusion fields using sensor measurements," in *Proc. 41st IEEE International Conference on Acoustics, Speech and Signal Processing (ICASSP'16)*, Shanghai, China, Mar. 2016.

[9] H. Pan, T. Blu, and P. L. Dragotti, "Sampling curves with finite rate of innovation," *IEEE Transactions on Signal Processing*, vol. 62, no. 2, pp. 458–471, Jan 2014.

[10] J. Murray-Bruce and P. L. Dragotti, "Solving physics-driven inverse problems via structured least squares," in *Proc. European Signal Processing Conference (EUSIPCO'16)*, Budapest, Hungary, Aug. 2016.

[11] S. Sahnoun, K. Usevich, and P. Comon, "Multidimensional ESPRIT: Algorithm, Computations and Perturbation Analysis," Aug. 2016, working paper or preprint. [Online]. Available: https://hal.archives-ouvertes.fr/hal-01360438

[12] I. Maravić and M. Vetterli, "Exact sampling results for some classes of parametric nonbandlimited 2-d signals," *IEEE Transactions on Signal Processing*, vol. 52, no. 1, pp. 175–189, Jan 2004.

[13] I. Khalidov, T. Blu, and M. Unser, "Generalized L-spline wavelet bases," in *Proceedings of the SPIE Conference on Mathematical Imaging: Wavelet XI*. SPIE, Aug 2005, pp. 1–8.

[14] T. Blu and M. Unser, "Approximation error for quasi-interpolators and (multi-) wavelet expansions," *Applied and Computational Harmonic Analysis*, vol. 6, no. 2, pp. 219–251, 1999.

[15] J. A. Uriguen, T. Blu, and P. L. Dragotti, "FRI sampling with arbitrary kernels," *IEEE Transactions on Signal Processing*, vol. 61, no. 21, pp. 5310–5323, Nov 2013.

[16] M. Unser, "Sampling-50 years after shannon," *Proceedings of the IEEE*, vol. 88, no. 4, pp. 569–587, April 2000.